Effect of Post-Weld Treatment on the Microstructure and Mechanical Properties of Austempered FeNiCr Steel Welded Joint

Septian Adi Chandra[1], *Dhany* Zulkarnaen[2], *Dedi* Pria Utama[2], *Rahadian* Roberto[2], *Muhammad* Yunan Hasbi[2], *Winarto*[1*], and *Fatayalkadri* Citrawati[2]

[1]Department of Metallurgical and Materials Engineering, University of Indonesia, Depok, Indonesia
[2]Research Centre for Metallurgy, National Research, and Innovation Agency, Tangerang Selatan, Indonesia

Abstract. This study investigated isothermally treated FeNiCr structural steel welded joints. The base metal contains various phases which are dominated by a mixture of bainite and martensite. Joining this steel can be challenging since it has high carbon equivalent values and high hardness. Shielded metal arc welding (SMAW) with austenitic stainless-steel electrodes is used to avoid cold cracking. After the welding process, the samples were subjected to three various post-weld temperatures: 425°C, 475°C, and 525°C. From the tensile test results, the tensile strength of welded joint shows an increase as the temperatures increase. The highest value is reached for a joint sample which treated at 525°C, with a tensile strength of 680 MPa. Conversely, the highest elongation is obtained by the 425°C post-treated sample, which is 14%. The microstructure in the weld metal (WM) area shows a formation of δ-ferrite, whereas the HAZ and BM areas show the presence of bainite and martensite tempered phases with various plate densities, plate size, and plate shapes depending on its post-treatment temperatures, which then affect the value of the hardness.

1 Introduction

Isothermally treated FeNiCr structural steel under studied can be classified into armour steel AISI 4130[1], AISI 4330V[2], AISI 4340[3], [4], Protac 500[5], or Armox 500T[6]. The previously mentioned group of steels is generally strengthened by quenching and tempering processes. They mostly have high strength (yield strength > 1100 MPa), high hardness (hardness > 390 BHN), and high carbon equivalent (CEIIW ≥ 0.5) [3], [7]. It is used in civil constructions and military structures, i.e., mortar shells, tank hulls, turret structured in armoured vehicles, battle tanks and helicopter components[1], [3], [6].

Welding is one of manufacturing processes used to join components made from armour steel. Among welding technique in arc-welding methods, shielded metal arc welding (SMAW) is suitable for joining armour steel. It is due to its capability for joining thick steel sections with lower cost and convenient equipment handling for reaching a wider area [1], [6]. A proper welding procedure is required to avoid problems which commonly encountered during the process, which are hydrogen-induced cracking (HIC) or cold cracking or delayed cracking, and loss of heat-affected zone (HAZ) hardness [7], [8].

The parameters that critically affect HAZ and fusion line(FL) susceptibility to HIC are an increasing amount of dissolved hydrogen and high hardness in the HAZ area near fusion line due to a volume increase of hard structure martensite[5].

There are several welding parameters can be applied to prevent HIC, one of them is by using a suitable consumable, it is either low hydrogen ferrite (LHF) or austenitic stainless steel (ASS) consumables. ASS consumable fillers metal is known for their good resistance to cold cracking. More dissolved hydrogen are permitted without cracking because the solubility of hydrogen in the austenitic phase is significantly larger and its diffusivity is lower than that of ferrite [5], [9]. In addition to consumable fillers metal, preheating and interpass temperature can be used to manage excessive hardness in HAZ near the fusion line by reducing the cooling rate.

During the welding process, HAZ will undergo changes in microstructure and creates residual stresses [10], therefore, tempering or post-weld heat treatment (PWHT) is used to improve the HAZ microstructure by changing the martensite and retained austenite phases to tempered martensite and bainite [2]. Studies on a welded high strength low alloy steel (HSLA) subjected to a PWHT at 400 to 650°C for either 1 or 2 hours [11]–[13] resulted grain structure becomes more uniform in HAZ and weld zone.

For FeNiCr alloys with bainite as its dominant structure, not many studies discussing on its welding properties. Therefore, this study aimed to observe the effect of PWHT on the integrity, the microstructure, and

*Corresponding author: winarto@metal.ui.ac.id

the mechanical properties of isothermally treated structural steel which was joined using SMAW technique and ASS filler.

2 Materials And Methods

2.1 Sample and Welding Preparation

The base metal (BM) sample used in this study is an as-cast FeNiCr steel plate. Prior to the joining process, the sample underwent a sequence of heat treatment process to obtain a bainite phase. It was first austenized at 950 °C then austempered at 475 °C followed by air cooling. The resulted microstructure of the BM sample is shown in **Fig. 1**. It is a multiphase microstructure with the present of bainite dark area and martensite light area in the mixture [14][15].

For the SMAW joining process, the BM plate was cut to a dimension of 12 x 60 x 150 mm. **Fig. 2a** shows the schematic image of multi-pass welded plate with SMAW process. **Fig. 2b** shows a single V-groove with 60° angle joint configuration and a root gap of 2 mm. The electrode used in the joining process was austenitic stainless-steel NC-39L welding wire. This electrode has yield strength of 410 MPa and tensile strength of 560 MPa. The chemical composition of this electrode, along with, the BM sample is listed in **Table 1**.

The parameters used during the welding process are listed in **Table 2**. It includes the parameters for pre-heating and post-heating of the joined sample. The pre-heating process used a muffle furnace. The temperature was monitored using a thermocouple wire and an infrared thermometer. Following the pre-heating, the sample then welded using an ESAB TA33 welding machine. The duration of each pass was measured using a stopwatch.

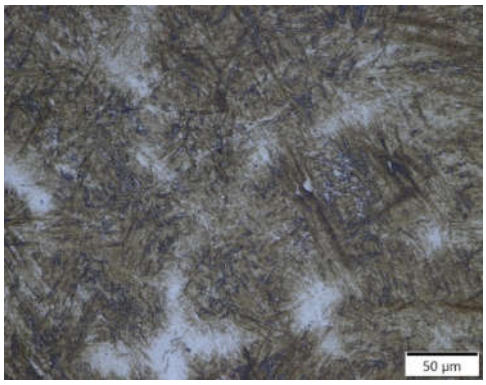

Fig. 1. Microstructure image of the as-cast BM sample prior to joining process. Etched with 4% picral.

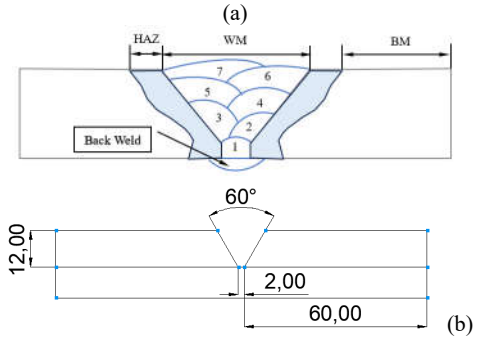

Fig. 2. The schematic images of (a) welding sequence and (b) joint configuration

Table 1. Chemical composition (wt.%) of base metal and welding electrode.

Material	C	Si	Mn	Al	P	S	Ni	Cr	Mo	Cu
BM	0,11	1,2	0,22	0,9	0,044	0,022	2,4	1,8	-	0,0071
NC-39L	0,04	0,42	1,6	-	0,03	<0,01	13,3	23,8	0,18	0,09

Table 2. Parameters used during the welding process.

Parameters (unit)	Sample Code		
	PWHT 425	**PWHT 475**	**PWHT 525**
Electrode (AWS E)	309-16L	309-16L	309-16L
Electrode polarity	DCEP	DCEP	DCEP
Welding position	1G	1G	1G
Preheat (°C)	150	150	150
InterPass (°C)	200	200	200
PWHT (°C)	425	475	525
Electrode baking (°C)	200	200	200
For Root Pass & Filling Pass Welding			
Electrode diameter (mm)	2.6 & 3.2	2.6 & 3.2	2.6 & 3.2
Welding current (A)	52 & 110 – 114	52 & 110 – 114	52 & 110 – 114
Arc voltage (V)	23-26	23-26	23-26
Welding Speed (mm/sec)	3.19 & 1.3	3.19 & 1.3	3.19 & 1.3

After the welded sample reached the martensite finish temperature, the sample was immediately undergoing a PWHT process at either 425 ℃, 475 ℃ or 525 ℃ for 30 minutes in a muffle furnace. The joined samples then named as sample PWHT 425, sample PWHT 475 and sample PWHT 525.

In order to check the soundness of the joint, after 72 hours of incubation, the welded samples then subjected to dye penetrant and X-Ray radiography non-destructive tests. The results showed no welding defects (e.g., surface, and internal cracks) were observed.

2.2 Mechanical Tests and Characterization

The mechanical tests and metallographic samples were prepared from all joined samples. For tensile test, the three samples were cut using a wire-cut machine to obtain a sub size plate sample as in ASTM E8. The weld metal (WM) area was placed in the center of the gauge length. The test was then conducted using a Tinius Olsen 300SL tensile machine.

The sample used for microstructure characterization and Vicker's hardness test was prepared through the same procedures. The cross-section part of each sample were ground and polished up to 1 µm. Both, microstructure observation and hardness test areas for each sample cover the WM area, the HAZ area, and the BM area.

The as-polished samples then etched to reveal the microstructure of each area. The 4% picral solution was used for the HAZ and the BM, and combination aqua regia and Kalling's for the WM area. The microstructure images then acquired using an Olympus BX-53 optical microscope.

For the hardness test, the data was taken using Mitutoyo HM-200 with 15 secs dwelling time and 1 N load. The test was performed according to ASTM E384-17 and ISO 9015-2:2015. The test area was 2 mm from the sample surface and the hardness data were collected start from the centreline in the WM area through the HAZ area and end in the BM area.

3 Results And Discussion

3.1 Microstructures

The microstructure of all Samples was observed with an optical microscope which was captured 2mm from the surface in 3 different areas namely Base Metal (BM), HAZ, and Weld Metal (WM). The WM from all Samples used AWS 309L has alloy on the Cr-rich with the ratio of equivalent chromium and nickel Creq/Nieq =1.6 so δ-ferrite is the primary solidification phase. The proportion of comparable nickel and chromium ratio of equivalent chromium and nickel Creq/Nieq is 1.3 to 1.6, the welds metal will contain a phase austenitic matrix with a small quantity of ferrite[16]. The chemical composition of the steel, namely the chromium to nickel ratio, significantly impacts the amount and distribution of δ-ferrite. The dark dendrites as shown in **Fig. 3**a-c are δ-ferrite types of morphology vermicular in an austenite matrix[3][17]. The massive δ-ferrite growth can increase the hardness and tensile strength in WM[5], [17], [18]. From the qualitative analysis of the phase area fraction in WM using image j software obtained 7.21%, 7.64%, and 8.13% area of δ-ferrite in the austenite matrix for samples PWHT 425, sample PWHT 475 and sample PWHT 525 respectively. All Samples had a proper percentage of δ -ferrite in the weld of the austenitic stainless steel. Too much δ -ferrite ≥10 vol % will reduce ductility, toughness, and corrosion resistance, while ≤5 % vol too little can cause solidification cracks.

The HAZ is close to the Fusion Zone (FZ), and it has a high enough temperature to allow for microstructure changes. The HAZ is divided into separate zones according to their peak temperatures and lengths of high temperatures: the coarse-grained HAZ (CGHAZ) and the fine-grained HAZ (FGHAZ). After welding untampered martensite from BM may get transformed into tempered martensite[8] and martensite or bainite phase[6]. This phase change is due to the heat energy during welding capable of heating CGHAZ to temperatures above the AC3 point or becoming the austenite phase. The cooling rate after welding also affects the BM phase changes in the HAZ. PWHT processing of the entire Sample was carried out immediately after welding when the temperature in the Sample exceeded the finished martensite. CGHAZ microstructure for all Samples was captured 500µm from the FL and consisted of a mixture of lath tempered martensite and bainite microstructures as shown in **Fig. 4**a-c by arrows with code letters LM and B[19]. The FGHAZ region likewise exhibits an observation that is comparable to that in the CGHAZ was captured 2mm from the FL. Sample PWHT 425 has a denser martensite phase distribution when com-pared to Sample PWHT 475 and Sample PWHT 525. Micro-

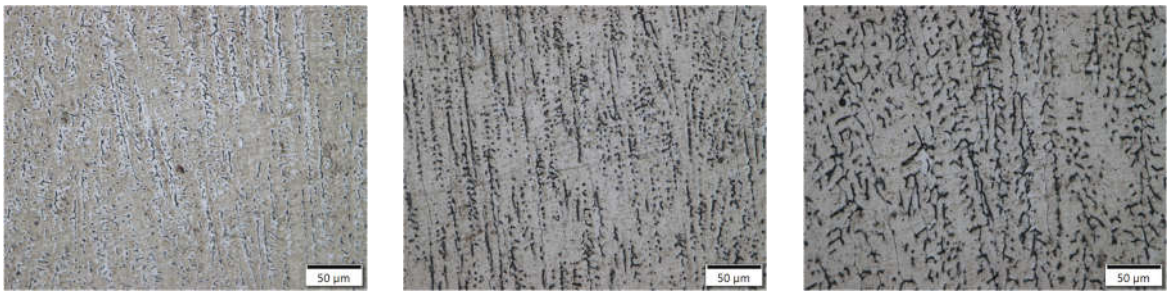

(a) (b) (c)

Fig. 3. Microstructure of WM areas for (a) sample PWHT 425, (b) sample PWHT 475, and (c) sample PWHT 525

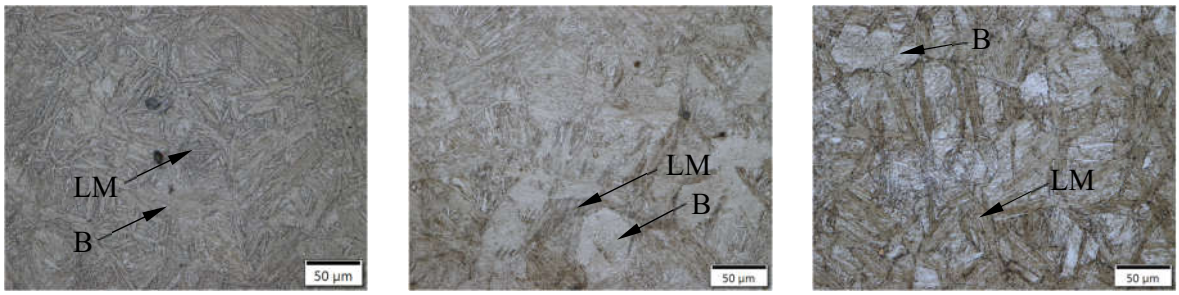

(a) (b) (c)

Fig. 4. Microstructure of CGHAZ areas for (a) sample PWHT 425, (b) sample PWHT 475, and (c) sample PWHT 525

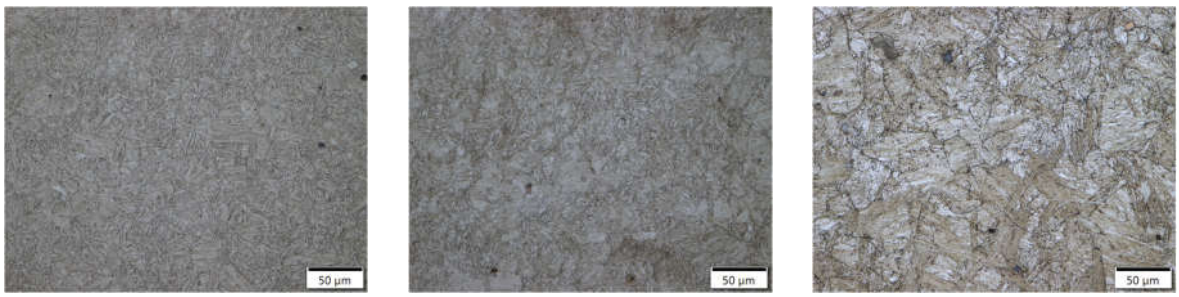

(a) (b) (c)

Fig. 5. Microstructure of FGHAZ areas for (a) sample PWHT 425, (b) sample PWHT 475, and (c) sample PWHT 525

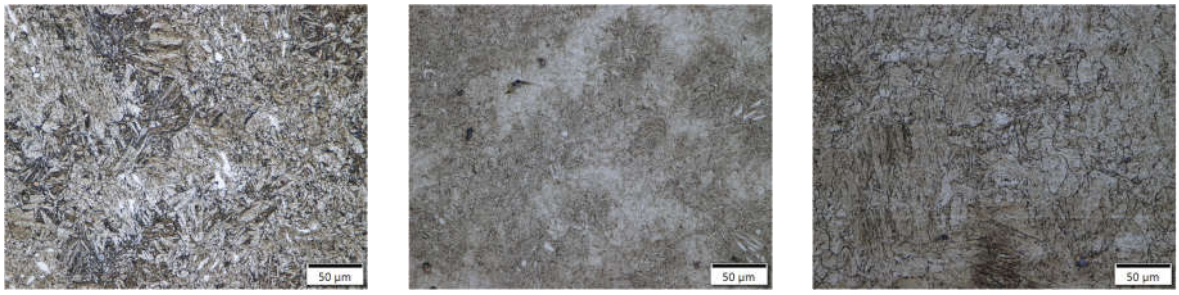

(a) (b) (c)

Fig. 6. Microstructure of BM areas for (a) sample PWHT 425, (b) sample PWHT 475, and (c) sample PWHT 525

structure in FGHAZ for all Samples in **Fig. 5** has the same morphology as CGHAZ but finer lath and grain size. Increasing the PWHT temperature increases the lath and grain size in CGHAZ and FGHAZ.

3.2 Hardness

The hardness profile of sample PWHT 425, sample PWHT 475, and sample PWHT 525 is presented in **Fig. 7**. From the centreline in the WM area to the fusion line, ~4.5 to ~5 mm from the centreline, the hardness distribution of the three samples is in the range of 175 to 200 VHN (**Fig. 7**(a)). The hardness variation among the three samples is not significant.

As the indentation move further from the fusion line, the hardness of the three samples increases significantly (**Fig. 7**(b)). This area has a different structure from the WM area and already considered as HAZ area. The width of the HAZ area is varied for each sample. For the CGHAZ area it lays at ~5 mm to ~7.5 mm from the centreline. In this area, the highest hardness in sample PWHT 425, sample PWHT 475, and sample PWHT 525 reach 456.5 ± 9.05 VHN, 438.3 ± 7.16 VHN, and 435.5 ± 5.09 VHN, respectively. The hardness variation in this area for each sample is minor. However, further from the centreline, in the FGHAZ area **(Fig. 7**(c)), the hardness distribution of sample PWHT 425, sample PWHT 475, and sample PWHT 525 shows a different trend. The hardness of these three samples is inversely proportional

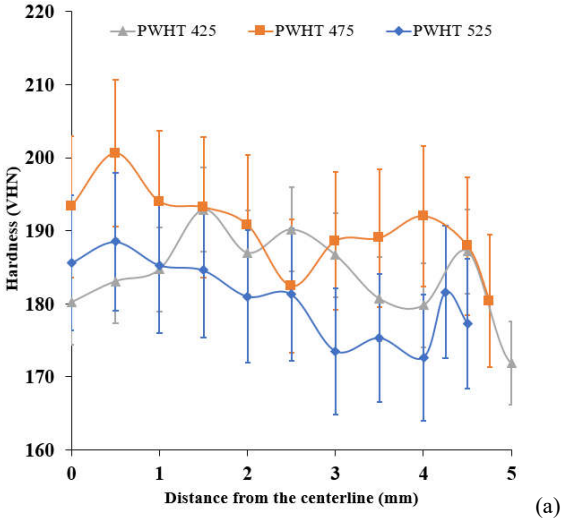

(a)

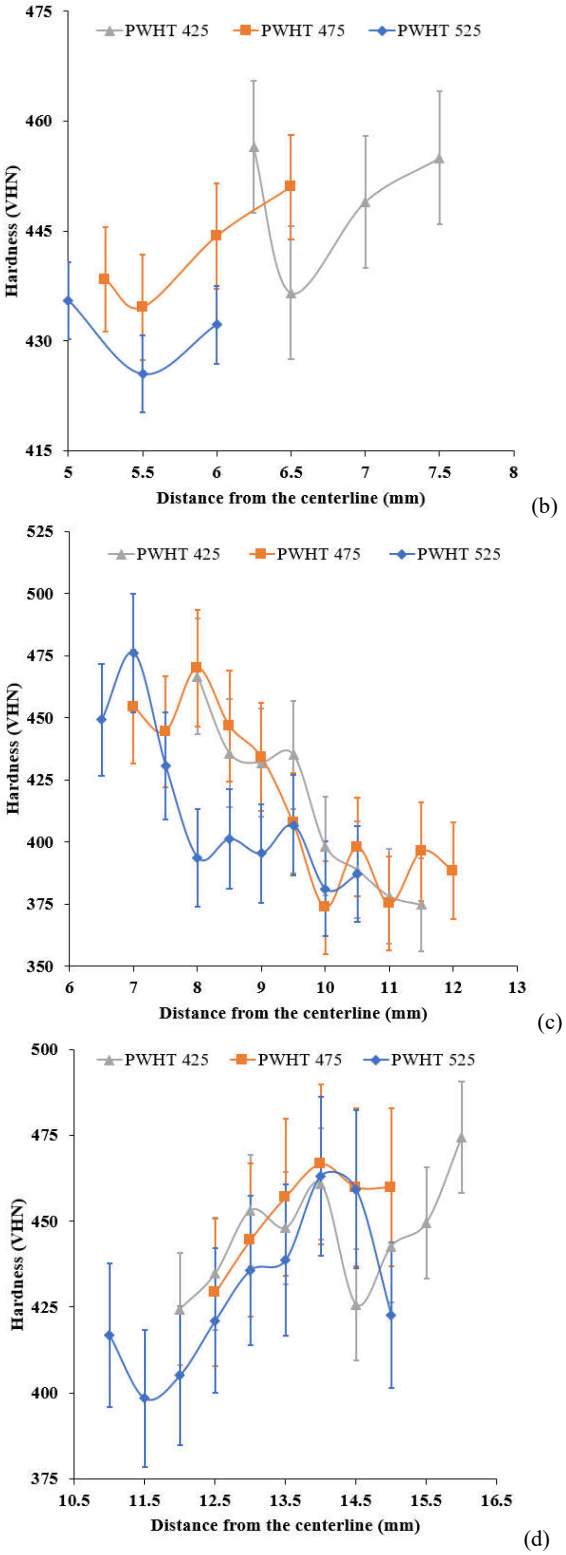

Fig. 7. Hardness distribution of the three samples along the (a) WM area, (b) CGHAZ area, (c) FGHAZ area, and (d) BM area measured 2 mm below the surface.

to the indentation distance. The hardness variation in this area is more substantial than the previous area, CGHAZ. The FGHAZ area spans from ~8 to ~11.5 mm for sample sample PWHT 425, ~7 to ~12 mm for sample PWHT 475, and and ~6.5 to ~10.5 mm for sample PWHT 525. The lowest hardness reaches at an indentation point close to the BM area, with a value of 374.8 ± 33.18 VHN, 373.8 ± 33.83 VHN and 381.2 ± 31.88 VHN for sample PWHT 425, sample PWHT 475, and sample PWHT 525, respectively.

In the BM area, the hardness trend of the three samples shows an uptrend (**Fig. 7**(d)). The BM area started at a distance of ~11 to ~12 mm and measured up to ~15 mm from the centreline. The variation of the hardness data in this area is not as high as in the FGHAZ area. But this hardness value is lower than the average hardness value before the joining process is 498.04 ± 9.00.

Among all areas, the fluctuation in hardness is more pronounce in FGHAZ followed by BM areas. This might be due to the distance of these two areas are further from the source of heat during welding. Therefore, this area subjected to heat and cold cycles at a shorter time compared to WM and CGHAZ areas.

Moreover, comparing between the hardness data and literatures, the three samples indicates the formation of bainite and martensite in the HAZ and BM areas[20], [21].

3.3 Tensile Strength

The fractured area of the three samples is depicted in **Fig. 8**. All samples show a necking in the WM area before fractured (**Fig. 8**(a), (c), and (e)). The fractured surfaces of the three samples show a dull area with a slight bright area at the edge of the sample (**Fig. 8**(b), (d), and (f)). It means that the fracture is considered as ductile which in accordance with the hardness of WM in **Fig. 7**(a).

The transverse tensile properties such as tensile strength and percentage of elongation of joints were evaluated. In each joint, three Samples were prepared and tested as presented in **Table 3**. BM has a greater tensile strength than the three joint strengths, namely 1650 MPa, this is because the connection process uses ASS electrodes.

Sample with a PWHT temperature of 425°C has a tensile strength of 594 MPa, showing a 64% reduction in strength from BM. Sample with a PWHT temperature of 475°C has a tensile strength of 629 MPa, showing a 62% reduction in strength from BM. Sample with a PWHT temperature of 525°C has a strength of 680 MPa which shows the lowest decrease in strength when compared to the other 2 samples, which is 59% of the BM. Sample

Table 3. Tensile strength test results of Base Metal and welding joints

Sample	σ_{UTS} (MPa)	Reduction strength (%)	Elongation to fracture (%)
BM	1650	-	11.33
PWHT 425	594	64	14
PWHT 475	629	62	11
PWHT 525	680	59	10.44

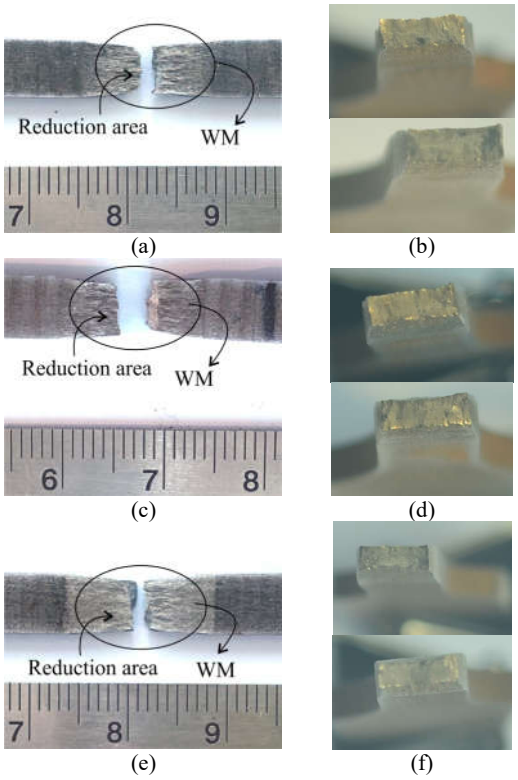

Fig. 8. Fracture location and fracture surface of (a), (b) sample PWHT 425, (c), (d) sample PWHT 475, and (e), (f) sample PWHT 525 after tensile test. All three samples fractured at the WM area.

PWHT 525 joints showed 7.6 and 12.7% higher tensile strength than Sample PWHT 475 and Sample PWHT 425. The elongation to fracture in the length of BM and the three Samples were 11.33%, 14%, 11%, and 10.44 %, respectively. In **Fig. 9**. shows the stress-strain curves on the three joining which are compiled from one of the samples from the test results of samples PWHT 425, PWHT 475, and PWHT 525.

Sample PWHT 525 showed the highest strength but the lowest elongation among the three Samples. This is related to the amount of δ-ferrite Sample PWHT 525 in the austenite matrix which is more than the others.

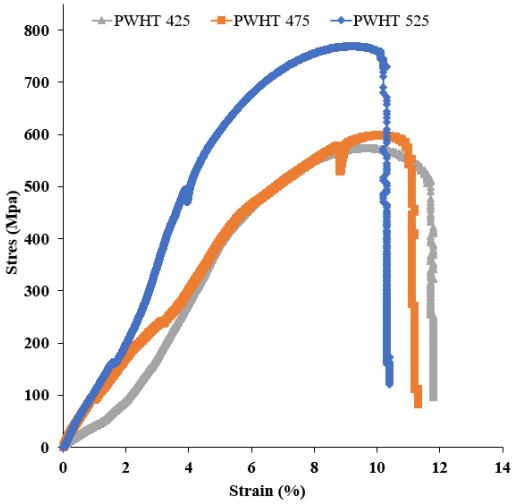

Fig. 9. Stress-Strain curves of sample PWHT 425, PWHT 475, and PWHT 525

Conclusions

The study has shown result of FeNiCr high strength low alloy steel welded joints. All of samples in weld metal area have vermicular δ-ferrite in austenite matrix microstructure with different distribution. The greater the number of δ-ferrite increases the hardness and tensile strength.

In the HAZ area, the three samples have tempered martensite and tempered bainite phases, sample PWHT 425 with the lowest PWHT temperature at 425°C has a higher density of martensite phase, smaller lath, and grain size. The hardness values of the CGHAZ and FGHAZ areas of sample PWHT 425 as measured from the centerline 6.25mm and 8mm are 456.5 HV and 466.6 HV are the highest micro hardness values.

All samples have a failure position in the WM area, after being tested for their tensile strength. Sample PWHT 525 with a PWHT temperature of 525°C has the highest tensile strength of the weld metal of 680 MPa but has the lowest elongation value of 10.44%.

Declaration of Competing Interest

The authors confirm that none of their known competing interests appeared to have an impact on the research presented in this study.

Acknowledgment

The National Research and Innovation Agency of the Republic of Indonesia, which supported this research, is acknowledged by the authors as being a supporter of their work.

References

1. N. V. Kumar, M. Uthayakumar, S. T. Kumaran, and A. Velayudham, Hum. Factors Mech. Eng. Def. Saf., **6**, pp 1-11(2022)
2. M. Zuk, J. Gorka, A. Czuprynski, and M. Adamiak, Metalurgija, **55**, pp. 613–616(2016)
3. V. Balaguru, V. Balasubramanian, and P. Shivkumar, World J. Adv. Eng. Technol. Sci., **1**, pp. 71–84(2020)
4. M. Balakrishnan, V. Balasubramanian, and G. M. Reddy, Key Eng. Mater., **812**, pp. 1–8(2019)
5. A. Cabrilo and K. Geric, Adv. Mater. Res., **1138**, pp. 79–84(2016)
6. A. Saxena, A. Kumaraswamy, G. Madhusudhan Reddy, and V. Madhu, Def. Technol., **14**, no. 3, pp. 188–195(2018)
7. P. Kah, M. Pirinen, R. Suoranta, and J. Martikainen, Adv. Mater. Res., **849**, pp. 357–365(2014)
8. G. Magudeeswaran, V. Balasubramanian, T. S. Balasubramanian, and G. M. Reddy, Sci. Technol. Weld. Join., **13**, pp. 97–105 (2013)
9. S. Alkemade, Def. Sci. Technol. Organ., p. 24, (1996)

10. S. Ghorbani, R. Ghasemi, R. Ebrahimi-kahrizsangi, and A. Hojjati-najafabadi, Mater. Sci. Eng. A, **688**, pp. 470–479(2017)
11. A. J. C. Gomes, J. C. F. Jorge, I. S. Bott, L. F. G. Souza, M. C. Mendes, and L. S. Araújo, Metallogr. Microstruct. Anal., (2019)
12. M. Khan, M. Washim, and Z. Sarkar, J. Manuf. Process., **64**, pp. 1307–1321(2021)
13. J. C. Ferreira Jorge, J. L. Dias Monteiro, A. J.de Carvalho Gomes, I. de Souza Bott, L. F. G. de Souzaa, Matheus Campolina Mendes, and L. S. Araújo, J. Mater. Res. Technol., **8**, pp. 561–571(2018)
14. G. F. Vander Voort, Heat Treating Progress, **9**, May (2001)
15. Committee ASM International, **9** p. 2733(2004)
16. T. Wegrzyn, Weld. Int., **6**, pp. 690–694(1992)
17. R. Ghasemi, B. Beidokhti, and M. Fazel-Najafabadi, Arch. Metall. Mater., **63**, pp. 437–443(2018)
18. P. V. Muterlle, M. Zendron, M. Perina, and A. Molinari, 20th Int. Congr. Mech. Eng., pp. 1–6, (2009)
19. M. Wu, Z. Luo, and S. Ao, J. Mater. Eng. Perform., (2023)
20. S. S. Hanza, B. Smoljan, L. Štic, and K. Hajdek, Metals (Basel), **11**, pp. 1–14(2021)
21. H. Zakerinia, A. Kermanpur, and A. Najafizadeh, International Journal of ISSI, **6**, pp. 14–18(2009)